1007-4619 (2012) 01-154-12 Journal of Remote Sensing 遥感学报

Ocean surface wind and wave monitoring at Typhoon Fung-Wong by HFSWR OSMAR071

LI Lun[1], WU Xiongbin[1], LI Yan[2], LONG Chao[1], LIU Bin[1], XU Xing'an[1], CHEN Min[3], XUE Chaoying[3]

1. *Electronic Information Institute of Wuhan University*, *Wuhan* 430079, *China*;
2. *State Key Laboratory of Marine Environment Science/ Xiamen University*, *Xiamen* 361005, *China*;
3. *International school of Software of Wuhan University*, *Wuhan* 430079, *China*

Abstract: This paper provides wind and wave observation results detected by high frequency surface wave radar OSMAR071 during Typhoon Fung-Wong. Methods for extracting ocean surface parameters from HFSWR sea echo are introduced. The Stewart Barnum and Maresca SBM method combined with multi-beam sampling method is used to invert wind direction. A modified Barrick's model is proposed to obtain significant wave height and the SMB formulation is used to extract wind speed information. Compared with buoy data of wind and wave, radar inversion results show good agreement with in-situ observations. The root-mean-square error RMSE of significant wave height, wind speed and wind direction between radar-derived and those from the buoy are 0.48 m, 3.5 m/s, 27.7°, and the coefficients of determination (R^2) are 0.72, 0.60 and 0.97, respectively. Factors affecting detecting accuracy are also discussed in this paper.

Key words: typhoon, high frequency surface wave radar (HFSWR), OSMAR071, significant wave height, wind field
CLC number: P716+.22 / TN958.93 **Document code:** A

Citation format: Li L, Wu X B, Li Y, Long C, Liu B, Xu X A, Chen M and Xue Y C. 2012. Ocean surface wind and wave monitoring at Typhoon Fung-Wong by HFSWR OSMAR071. Journal of Remote Sensing, 16(1): 154–165

1 INTRODUCTION

As China is located at western bank of the Pacific Ocean, the typhoon is a frequent issue. With the varieties of global climate, the frequency of typhoon and typhoon-caused disasters all present trends of escalation. At present, the typhoon surveying methods are limited, mainly by in-situ observations, from numerical simulations and remote sensing. It is difficult and expensive to measure typhoon by buoy, dives tools or research ship, and also limited partial spot or on-line data of special time can be obtained, which cannot reflect the real sea state of large area and cannot satisfy the oceanographic engineering and the marine forecasting demands. The numerical simulation results cannot completely represent the spatial structures of the sea wind or wave field. Study of typhoon is restricted by the limited typhoon observation methods. With more than 40 years' development, High Frequency Surface Wave Radar (HFSWR) operated in the HF band (3—30 MHz), employs the ground wave mode of radio wave propagation where the radar signal is guided by a good conducting surface such as the ocean surface to follow a path that essentially matches the Earth's curvature. It is capable of all-weather remote sensing of large area ocean surface dynamics with relatively high precision (Barnes, 1998). Its capability of currents detection has been considered satisfying the requirements for routine marine observations while its wind and wave measurements cannot provide engineering applications (Barrick, 2008; Wu, et al., 2003; Liu, et al., 2007). Observation ocean surface wind and wave field at typhoon by HFSWR is a new remote sensing technology. OSMAR071 is the latest product of Ocean State Monitor and Analysis radar (OSMAR) series of HFSWR which is developed by the Radiowave Propagation Laboratory (RPL) of Wuhan University. It demonstrates high signal quality and engineering reliability compared with the prototype OSMAR and offers a good platform for the study of extracting ocean wave parameters from the second-order spectra of sea echoes. Recently, OSMAR071 system has made certain breakthrough in the wind and wave survey. Compared with buoy in-situ observations in nearly half one year time, results show that the RMSE difference between radar-derived significant wave heights and those from the buoy is 0.39 m and the coefficients of determination between the two series is 0.67 (Wu, et al., 2003). From 2008-07-28 to 2008-07-29, Typhoon Fung-Wong came across the north of Taiwan Straits, and the OSMAR071 observation sites located at Longhai and Dongshan in Fujian Province

Received: 2010-11-18; **Accepted:** 2011-04-29
Foundation: National High Technology Research and Development Program of China (863 program) (No. 2009AA09A301); National Natural Science Foundation of China (No. 60571065)
First author biography: LI Lun (1986—), male, Ph.D. candidate, he majors in HF radio marine remote sensing. E-mail: lilunhp@163.com
Corresponding author biography: WU Xiongbin(1968—) ,male, professor, his research interests are radio wave propagation and ocean remote sensing. E-mail: xbwu@whu.edu.cn

of China went through the terrible disaster and got all the on time current, wind and wave data of the sea area at the typhoon duration. This paper presents the wind and wave measurement at Typhoon Fung-Wong, and compares the results with in-situ observations.

2 METHOD

2.1 OSMAR071 system

OSMAR071 applies the Frequency Modulated Interrupted Continuous Wave (FMICW) waveform with 30 kHz bandwidth. A three-element Yagi-Uda antenna serves as transmitting antenna and an 8-element non-lineable receiving array as the radar antenna filed (Fig. 1). The major characteristic parameters of OSMAR071 are shown in Table 1. Array amplitude and phase correction is obtained by real-time software calibration. A Fast Flourier Transform (FFT) process is used by every pulse-repetition-interval PRI which we call a snapshot to produce a Range spectrum. After coherent accumulation at the same range, a second FFT is used to produce Range Doppler Power Spectrum. Fig. 2 shows the measured Range Doppler Power Spectrum of 1024 PRI coherent accumulation, which is from Longhai NO.2 receive antenna. From Fig. 2, we can see that a typical HFSWR sea echoes' Range Doppler Power Spectrum contains two nearly symmetrically located first-order peaks, second-order continuous spectral points, the obvious distance belt distributed ionosphere reflection echo, the obvious frequency belt distributed radio frequency interference, ship echo and the noise floor. The Multiple Signal Characteristic (MUSIC) algorithm is applied to discern the direction of arrival (DOA) of sea echoes. The Digital Beam Forming (DBF) is used to obtain the direction of Range Doppler Power Spectrum.

Fig. 1 Antenna array field of HFSWR OSMAR071

Table 1 The characteristic parameters of OSMAR071

Paramerter	Value
Work frequency / MHz	7.5—8.5
Mean transmitting power /W	150
The maximum range / km	200 (currents, wind direction) 100 (wind speed, wave height)
Range resolution/km	5
Coverage bearing scope/(°)	150
Azimuth resolution/(°)	1.5 (currents), 5(wind, wave)
Result temporal resolution/min	10 (Current field) 30 (wind and wave field)

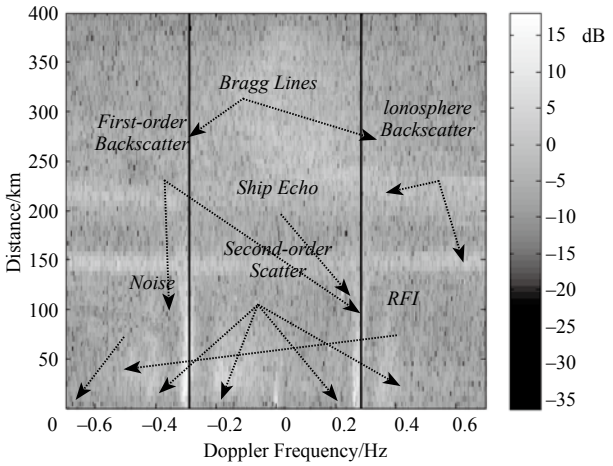

Fig. 2 Range doppler power spectrum of OSMAR071 (12:00, 2008-07-28)

2.2 OSMAR071 ocean surface parameters inversion

Based on the first-order sea echo radar cross section (RCS) derived by Barrick, the ocean surface current can be extracted by the dispersion relation of gravity wave in deepwater. The radial current can be obtained by one shore-based radar. As two radars detecting the same area from different directions at the same time, vector current can be synthesized. Several field experiments show that the ocean surface current information extracted from OSMAR series HFSWR can be applied in routine observations (Wu, et al., 2003).

The difference between the positive and negative first order sea echo Doppler spectrum peeks have close relationship with the wind direction which is formulated as a SBM model derived by Stewart and Barnum (1975):

$$R_d = 10\lg[\tan^s(|\theta_W|/2)] \quad (1)$$

where R_d is the ratio of the positive and negative first order wave energy, s is the value of spreading parameters which determines the wind energy disperse degree, θ_W is the wind direction from radar beam direction. The wind direction obtained by Eq. (1) is $\phi_W = \phi_0 \pm 2\arctan[10^{R/(10s)}]$, where ϕ_0 is the radar beam direction. The symbol "±" indicates the ambiguity in the deduced wind direction. The same wind direction to the radar beam direction is equivalent to the first order energy which causes the wind direction ambiguity. Finding wind direction by multi-beam sampling method proposed by Heron and Rose(1986) can be used to avoid wind direction ambiguity which assumes that the ocean wave spectral in the observation area is a uniform distribution approximately and by using different radar beam azimuths to observe corresponding ratios R_d. The ambiguity removal by switching radio beam direction relies on the assumption of an approximately uniform wind direction over area of ocean being observed. Fig. 3 gives the principle diagram of obtain wind direction by three radar beam directions.

The significant wave height information can be extracted from the continuous second order sea echo Doppler spectrum.

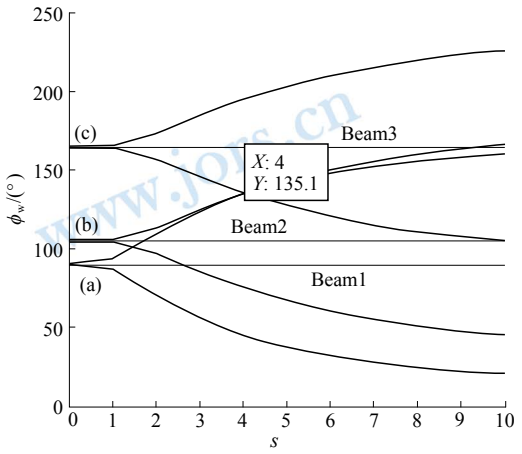

Fig. 3 Schematic diagram of three radar beam sampling method

In 1977, Barrick proposed a significant wave height inversion model which demonstrates robust applicability. A modified Barrick's model is proposed by Wu and Li (2009) to invert significant wave height from OSMAR071.

$$h = \frac{\alpha}{k_0}(R-\mu)^{\beta} \tag{2}$$

where R is the direct ratio of second-order power to that of the first-order power, k_0 is the radar wave number, α, β and μ are parameters of OSMAR071 which are 1.43, 0.71, and 0.4 using dataset from half one year experiments. The detailed description can be found in Wu, et al. (2009).

Proposed by Sverdrup and Munk and modified by Bretschneide, the SMB function gives the principle relationship of wind speed and significant wave height (Dexter & Theodorides, 1982) from which we can obtain wind speed by nonlinear iteration:

$$\frac{gH_S}{V_{10}^2} = 0.26\tanh\left[\left(\frac{1}{f_m V_{10}}\right)^{3/2}\frac{(3.5g)^{3/2}}{10^2}\right] \tag{3}$$

where H_S is ocean significant wave height, f_m is the peek frequency of ocean wave non-directional spectral, U_{10} is the wind speed at 10 m above sea surface and g is acceleration of gravity which equals to 9.8 m/s^2.

3 REMOTE MEASURING RESULTS AND ANALYSIS

3.1 Description of Typhoon Fung-Wong

Fung-Wong is the typhoon No.8 of the western north Pacific, generated in the east of Taiwan province over the ocean (130.6°E, 21.6°N) at 14:00, 2008-07-25. Then, it moved to the northwest steadily, intensified into severe tropical storm at 16:00, 2008-07-25, and then strengthened into typhoon in the afternoon while moving steadily to the west, and at 20:00 July 27 transformed into severe typhoon whose biggest wind power reached 45 m/s near the center. Around 6:30, 2008-07-28, it landed on Hualian in Taiwan province, and landed again on Donghai Town of Fuqing in Fujian province. It faded when entered into Shandong province.

3.2 Remote sensing of ocean surface wind and wave

OSMAR071 was located in Longhai in Fujian province which was in the radius of the gust of 7. During the Typhoon Fung-Wong landed on the Taiwan Straits and Fuqing of Fujian Province, the working frequency of radar was 7.82 MHz, while the corresponding resonant first-order scattering wave length was 19 m, and the Bragg frequency was 0.28 Hz. The range and azimuth resolution of the radar was 5 km and 5°, respectively. By weighted averaging the Doppler spectrum of the 3 (range cell)×3(azimuth cell) = 9 grid points, the wind and wave parameter inversion of the central grid point can thus be performed. Fig. 4 and Fig. 5 show the distribution of ocean surface wind and wave fields at 00:00, 6:00, 12:00, 18:00, 2008-07-28, respectively. In Fig. 4, the wave height of the northeast on the illuminated sea area of the radar was relatively high, which is consistent to the fact that the center of the typhoon was just in the northeast of the illuminated area. The tendency that the detected wave length ascended first and then descended is exactly in line with the time when the typhoon first landed on Taiwan Straits and then Fuqing of Fujian Province. Since tycoon is in low pressure, that is, the central air ascends and the sideward will complement the vacancy, the air turns out to be in a way of counterclockwise cyclone influenced by the deflecting force of earth rotation. The radar station was located in the southwest of the typhoon center, so during the typhoon center moving across northern Taiwan Straits, the wave direction of the illuminated area transformed from north to northwest, which is consistent with the features of wind direction displayed in Fig. 4. Besides, the features of wind velocity in Fig. 5 agree with those of wave height.

3.3 Analysis of measuring accuracy

The qualitative analysis in Section 3.2 indicates some insights. The ocean surface remote sensing results of OSMAR071 have satisfied the varying features of ocean surface wind and wave fields. In order to qualitatively verify the OSMAR071's measuring accuracy of wind and wave, results of radar's observations are compared to the wind and wave data of the big buoy in-situ observation nearby. Fig. 6 and Fig. 7 are comparisons and scatter diagrams of valid wave height time series by the radar and the buoy respectively during the Typhoon Fung-Wong. The correlation coefficient and the root mean square error (RMSE) are 0.72 and 0.48 m, respectively. Fig. 8 is the comparisons of time series of wind direction and wind velocity. Fig. 9 shows the scatter diagram of wind vector. The correlation coefficient and RMSE of wind direction are 0.97 and 27.7°, respectively. The correlation coefficient and RMSE of wind velocity are 0.6 and 3.5 m/s, respectively. The buoy went wrong since 12:00, 2008-07-29, so the real data of wind velocity was inaccessible.

According to the comparison results, the radar remote measuring results of the typhoon coincide with the buoy observation results, but there remains variance to some extent, and the reasons of the variance mainly lie in several respects:(1) Two detecting methods

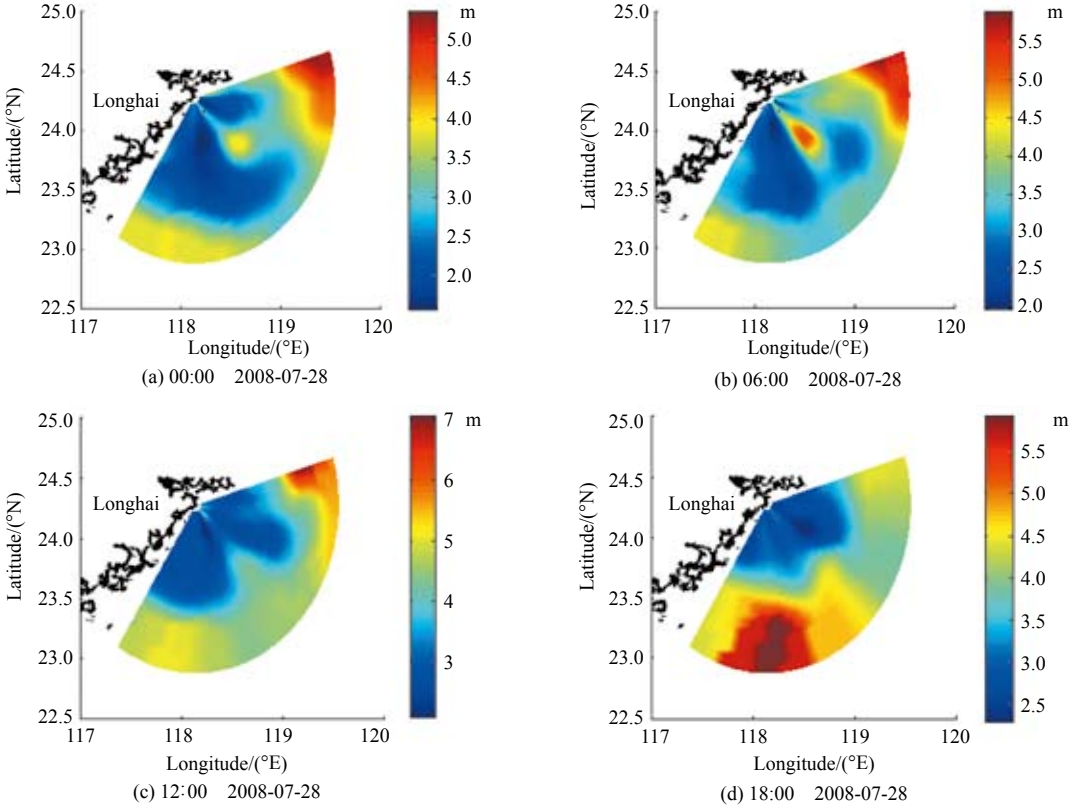

Fig. 4 Detected ocean surface wave height during Typhoon Fung-Wong by OSMAR071

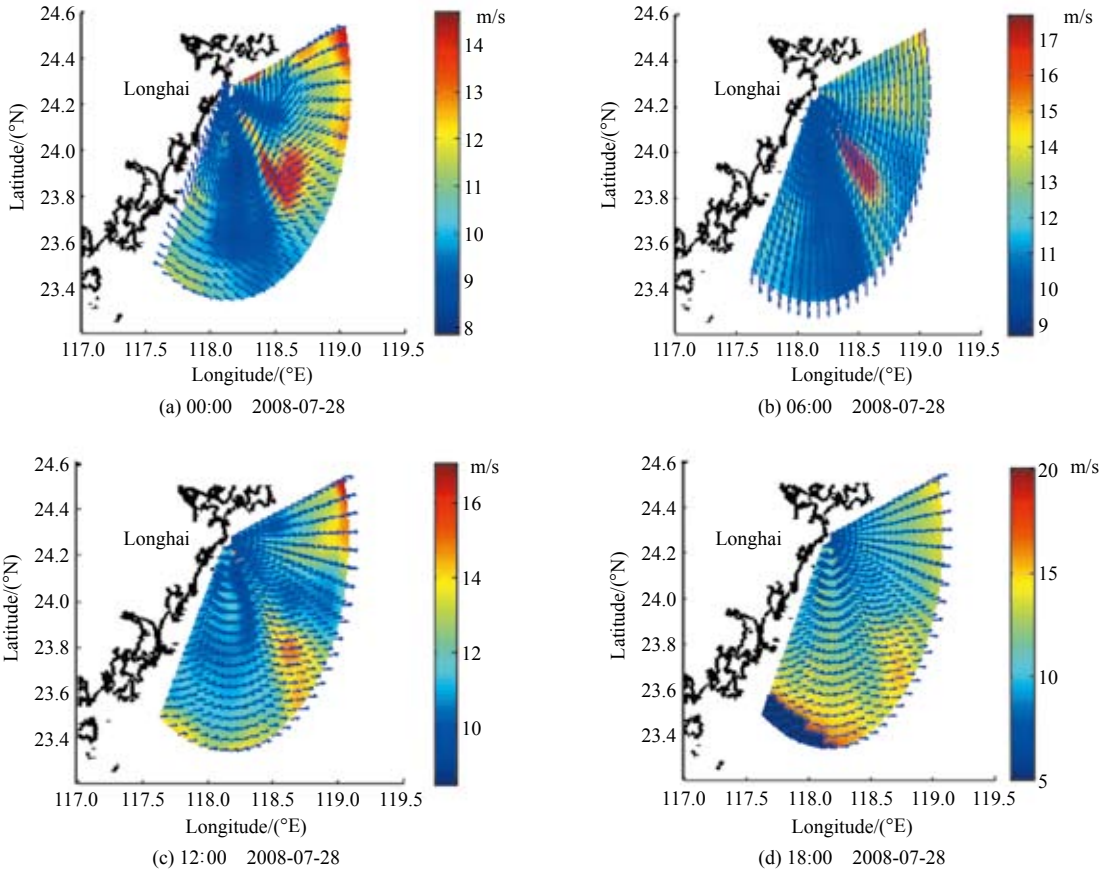

Fig. 5 Detected ocean surface wind field during Typhoon Fung-Wong by OSMAR071

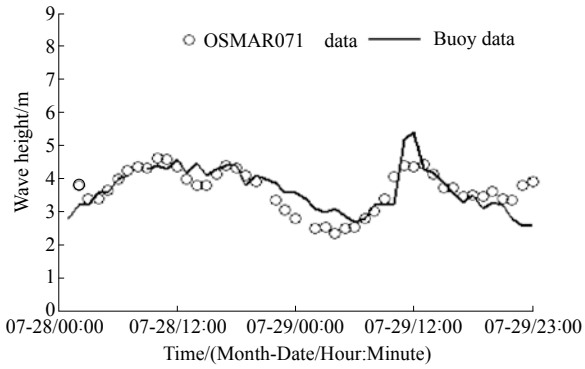

Fig. 6 Comparison of wave height time series between the radar and buoy (Time: 2008-06-28—29)

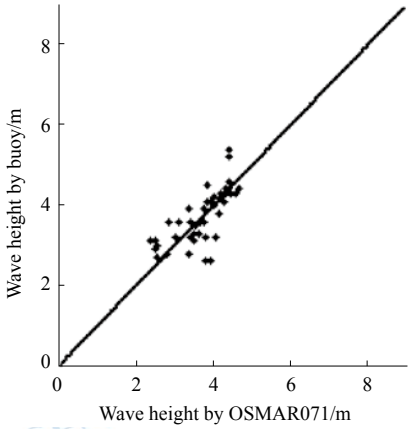

Fig. 7 Scatter diagram corresponding to the wave height series in Fig. 6

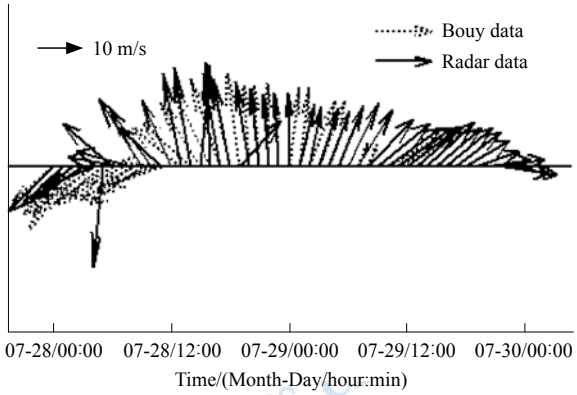

Fig. 8 Comparison of wind vector time series between the radar and buoy (Time: 2008-07-28—29)

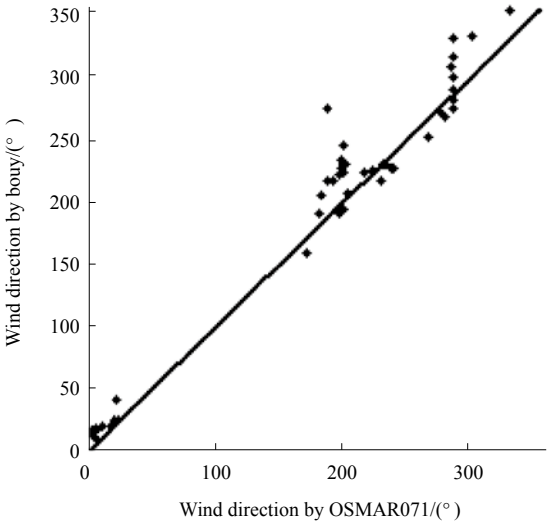

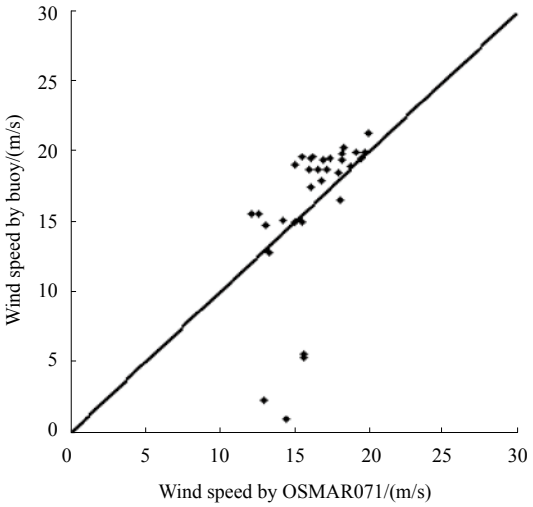

Fig. 9 Scatter diagram corresponding to the wind vector series in Fig. 8

are different in the sampling modes spatially and temporally. Radar averages the wave field data during from several square kilometers during tens of minutes, while buoy samples from the local wave height, which results in the variance. (2) Radar observation results are easily interfered by the complex electromagnetic environment (radio frequency interference (RFI)), hard targets such as ships on the sea, and ionosphere echo. (3) In high sea states, the strong high-order nonlinearity can make the edge between the first-order and the second-order sea echo spectrum blur and difficult to distinguish. (4) The inversion of valid wave height and wind velocity by HFSWR has depended on the SNR of second-order spectrum in the Radar echo spectrum to a large extent. The antenna's sidelobe and beam will affect the second-order spectrum. (5) During processing the echo spectrum, the average number of grid points, analysis of FFT spectrum and noise of the echo spectrum will definitely affect the inversion of wind and wave parameters. (6) The inversion model of wind direction is a binary nonlinear function, and the accuracy of wind direction measuring can be influenced by the error of the positive and negative first-order energy ratio and the error of extended wind direction factor. Several data of radar beam direction have been used to eliminate ambiguous wind directions in the study. In fact, the extended wind direction factor varies from different beam directions. And the low SNR, external RFI and the echo of hard targets like ships can also cause selecting fuzziness, leading to misjudgments. All these facts can affect the inversion accuracy of wind direction. In Fig. 9, at 21:00, 2008-07-28, there is an abnormal point resulted from ambiguous judgement of wind direction. From the sea echo Doppler spectrum, we can see fairly severe spectrum splitting, and it is possible that the echos of hard

targets like ships polluted the first-order sea echo, which leads to wind direction misjudgement.

In Fig. 9, the deviation becomes larger when the wind velocity measured by the buoy is smaller, because after 4:00, 2008-07-29 the buoy went wrong, which leads to unreliability of the data. In fact, it is a prevailing phenomenon of the foreign radars in low frequency that smaller wind velocity produces the larger errors. Its main reasons involve: (1) HFSWR measures the parameters of dynamics through remote sensing the resonant wave, and the wavelength of resonant wave is half that of radio wave. Between 7.5 and 8.5 MHz, the wavelength of resonant sea wave is about 20 m, and the wave fails to get sufficient energy to develop so that the echo is relatively weak and of poor stability, which leads to poor results. (2) The mechanism of HFSWR remote sensing of the ocean indicates that a lower radio wave frequency is suitable for detection of high sea states, while a high radio wave frequency is suitable for detection of low sea states. Consequently, part of the wind and wave detection problems in low sea states can be solved through matching the high and low end frequency to remote measure the sea surface simultaneously. But the attenuation of a high end frequency is severe, which results in the reduction of detection range and restriction of illuminated areas. (3) Another reason of the increase of observation errors with small wind velocity is unscientific, that is, when the wind and wave is small, a large number of inshore fishermen head out with their vessels among which themselves and the HF radio wave communication can cause interference and decrease the accuracy of the results.

4 CONCLUTION

The ocean wave spectra scope detected by HFSWR is limited by the applied radio wave frequency. In high sea conditions the low radio frequencies are needed in order to make wave measurements whereas in low sea conditions, higher radio frequencies are required. The OSMAR071 operates at 7.5—8.5 MHz which belongs to low radio frequency and the wavelength of corresponding ocean wave which can cause Bragg resonant scattering is nearly 20 m, thus radio wave at this frequency band are not sensitive to low sea condition and are suitable for high sea conditions monitoring. The sea state is relatively high at the period of typhoon which offers a proper opportunity for HFSWR wind and wave measurement study. It gives validation of wind and wave measurements from HFSWR OSMAR071 through the remote sensing at Typhoon Fung-Wong and results compared to buoy in-situ observations, which is the first time for measuring all time wind and wave at typhoon with wide spread by HFSWR in China. HFSWR which is located on the coast, measures ocean wind and wave extended to more than 100 km offshore and 200 km for wind direction measurements, which is more convenient than buoy in-situ observations. Offshore HFSWR, which is located on the coast of the ocean, easy to maintain and not influenced by inclement weather is a new remote sensing technique for ocean surface parameters observation at the period of typhoon.

Studies on extraction of waves and winds information from HFSWR is still under development. More work should be done to enhance the stability and accuracy of the wind and wave measurements. Moreover, the radar ocean echoes contain the ocean surface parameters such as wind direction, wind speed, wave height, wave direction and wave period, which can be extracted from ocean wave spectrum, and the radar range Doppler spectrum is characterized the interaction of radio wave and ocean gravity wave. Therefore, inversion the ocean wave spectrum from HFSWR range Doppler spectrum (Lipa & Barrick, 1986; Wyatt, 1986; Howell & Walsh, 1993; Hisaki, 2009), especially at the period of typhoon is the main work in the future.

Acknowledgements: Thanks to the State Key Laboratory of Marine Environment Science of Xiamen University for providing the buoy data.

REFERENCES

Barrick D E. 1977. Extraction of wave parameters from measured HF radar sea-echo Doppler spectra. Radio Science, 12(3): 415–424

Barrick D E. 2008. 30 Years of CMTC and CODAR. Proceedings of the IEEE/OES/CMTC Ninth Working Conference on Current Measurement Technology: 131–136

Barnes L. 1998. HF Radar-The Key to Efficient Wide Area Maritime Surveillance. EEZ Technology, Edition 3. London: ICG Publishing LTD: 115–118

Dexter P E and Theodorides S. 1982. Surface wind speed extraction from HF sky-wave radar Doppler spectra. Radio Science, 17(3): 643–652

Heron M L and Rose R J. 1986. On the application of HF ocean radar to the observation of temporal and spatial changes in wind direction. IEEE Journal of Oceanic Engineering, 11(2): 210–218 DOI: 10.1109/JOE.1986.1145173

Hisaki Y. 2009. Quality control of surface wave data estimated from low signal-to-noise ratio HF radar Doppler spectra.Journal of atmospheric and oceanic technology.26: 2444–2661

Howell R and Walsh J. 1993. Measurement of ocean wave spectra using narrow-beam HF radar. IEEE Journal of Oceanic Engineering, 18(3): 296–305

Lipa B J and Barrick D E. 1986. Extraction of sea state from HF radar sea echo: mathematical theory and modeling, Radio Science, 21(1): 81–100 DOI: 10.1029/RS021i001p00081

Liu L, Wu X B, Chen F, Yang S L and Ke H Y. 2007. Algorithm for HF radar vector current measurements. Journal of Oceanography, 63(1): 47–66 DOI: 10.1029/RS021i001p00081

Stewart R H and Barnum J R. 1975. Radio measurements of oceanic winds at long ranges: an evaluation. Radio Science, 10(10): 853–857 DOI: 10.1029/RS010i010p00853

Wu X B, Li L, Shao Y X, Li Y and Guo T. 2009. Experimental determination of sinificant waveheight by OSMAR71: comparison with results from Buoy. Journal of Wuhan University Nature Science, 14(6): 499–504

Wu X B, Yang Z L, Cheng F, Wu Z C, Yang Z J, Wen B Y, Shi Z F, Tian J S, Hou J C, Ke H Y and Gao H T. 2003. Ocean surface currents detection at the eastern china sea by hf surface wave radar. Chinese Journal of Geophysics, 46(3): 340–346

Wyatt L R. 1986. The measurement of the ocean wave directional spectrum from HF radar doppler spectra. Radio Science, 21(3): 473–485

“凤凰”台风期间海面风、浪的高频地波雷达OSMAR071遥感

李伦[1]，吴雄斌[1]，李炎[2]，龙超[1]，刘斌[1]，徐兴安[1]，陈珉[3]，薛超英[3]

1. 武汉大学 电子信息学院，湖北 武汉 430079；
2. 厦门大学 近海海洋环境国家重点实验室，广东 厦门 361005；
3. 武汉大学 国际软件学院，湖北 武汉 430079

摘 要：介绍了OSMAR071高频地波雷达系统“凤凰”台风期间海面风、浪遥测结果。文中给出高频地波雷达OSMAR071风、浪反演算法：利用SBM模型结合多波束采样法反演风向；利用改进的Barrick模型进行有效波高的反演；利用SMB关系式进行风速反演。将雷达定点观测结果与浮标数据进行对比，表现出很好的一致性，其中有效波高相关系数为0.72，均方根误差为0.48 m，风向相关系数为0.97，均方根误差为27.7°，风速的相关系数为0.6，均方根误差为3.5 m/s。文中还对影响探测精度的因素进行了分析。

关键词：台风，高频地波雷达，OSMAR071，有效波高，风场

中图分类号：P716+.22/ TN958.93 **文献标志码**：A

引用格式：李伦，吴雄斌，李炎，龙超，刘斌，徐兴安，陈珉，薛超英. 2012. “凤凰”台风期间海面风、浪的高频地波雷达OSMAR071遥感. 遥感学报，16(1): 154–165

Li L, Wu X B, Li Y, Long C, Liu B, Xu X A, Chen M and Xue Y C. 2012. Ocean surface wind and wave monitoring at Typhoon Fung-Wong by HFSWR OSMAR071. Journal of Remote Sensing, 16(1): 154–165

1 引 言

中国地处太平洋西岸，台风活动频繁。随着全球气候的变化，台风暴发频率及其造成的危害都成上升趋势。目前观测台风的手段非常有限，主要以现场观测，数值模拟和无线遥感为主。对于海上台风，利用浮标、潜标和海洋调查船等工具来测量，作业困难，费用大，而且往往只能得到特定时间内的局部点、线上的数据，无法反映待测海域的真实海况，不能满足海洋工程和海洋预报的需求；数值模拟结果也并不能完全代表海面风、浪场的空间结构。有限的台风观测手段制约了对台风的研究。近40年发展的高频地波雷达利用短波(3—30 MHz)在导电海洋表面绕射传播衰减小的特点，采用垂直极化天线辐射电波，能超视距探测海面流场、风场和浪场参数分布，实现对海洋环境大范围、高精度和全天候的实时观测(Barnes，1998)。目前主要地波雷达的海流探测已达到可用于常规业务化海洋观测水平(Barrick，2008；吴雄斌 等，2003；Liu 等，2007)，海浪、风参数的探测方面有待突破。利用高频地波雷达对台风期间海面风场和浪场进行观测是一种廉价低风险的遥感手段。

在武汉大学电波传播实验室研制的OSMAR系列高频地波雷达基础上改进的OSMAR071在雷达回波信号质量和系统工程可靠性方面比原工程样机都有了很大提高，为从雷达回波谱中提取有效波高和风速信息提供了很好的平台。近期，OSMAR071系统在风浪探测中取得了一定突破，近半年的试验观测表明雷达反演的有效波高值与浮标有效波高数据时间序列的均方根差为0.39 m，二者的相关系数为0.67(吴雄斌 等，2003)。2008年7月28日—29日，“凤凰”台风经过台湾海峡北部，福建龙海和东山站OSMAR071高频地波雷达经受住了恶劣天气的严峻

收稿日期：2010-11-18；**修订日期**：2011-04-29

基金项目：国家高技术研究发展计划(863计划)(编号: 2009AA09A301)；国家自然科学基金(编号: 60571065)

第一作者简介：李伦(1986—)，男，博士研究生，现从事高频地波雷达海洋环境参数遥感研究。E-mail: lilunhp@163.com。

通信作者简介：吴雄斌(1968—)，男，教授，博士生导师，主要研究方向为无线电波传播和无线电海洋遥感，发表论文50余篇，专利和软件著作权20余项。E-mail: xbwu@whu.edu.cn。

考验，完整获取了整个台风期间该海域的风、浪、流的观测数据。本文介绍了OSMAR071系统在台风期间的风、浪观测情况，并将该数据与浮标观测数据进行对比，表现出较为满意的一致性。

2 研究方法

2.1 OSMAR071系统

高频地波雷达OSMAR071系统是采用线性调频中断连续波(FMICW)体制的宽波束雷达，工作带宽为30 kHz，发射天线为三元八木天线，接收天线为八元非线性阵列，图1为该雷达天线场地。表1给出了该系统的主要技术参数。该雷达利用海洋回波对阵列通道幅度和相位进行软件实时在线校正；经过每个扫频周期回波的，快速傅里叶变换(FFT)得到距离谱，对每个距离的回波数据进行相干积累后进行第二次FFT就可以得到回波多普勒谱。图2为龙海站第2号接收天线实测雷达回波数据经过1024个扫频周期积累后得到的随距离分布的多普勒谱，从该谱图上可以明显的看到HFSWR回波多普勒谱由Bragg频率附近近似对称的一阶后向散射回波、连续的二阶散射回波、具有明显距离带分布的电离层回波、具有明显频率带分布的射频干扰回波、舰船回波和基底噪声等组成。利用Multiple Signal Characteristic(MUSIC)算法来实现对信号波达方向Direction of Arrival(DOA)的超分辨估计；通过Digital Beam Forming(DBF)可以得到覆盖范围内各个波束方向的多普勒谱。

图1 高频地波雷达OSMAR071天线场地

表1 高频地波雷达OSMAR071基本参数

参数名称	性能指标
工作频率/MHz	7.5—8.5
平均发射功率/W	150
最大探测距离/km	200(海流，风向) 100(风速，波高)
距离分辨率/km	5
波束宽度/(°)	150
方位分辨率/(°)	1.5(海流)，5(风，浪)
结果时间分辨率/min	10(海流) 30(风，浪)

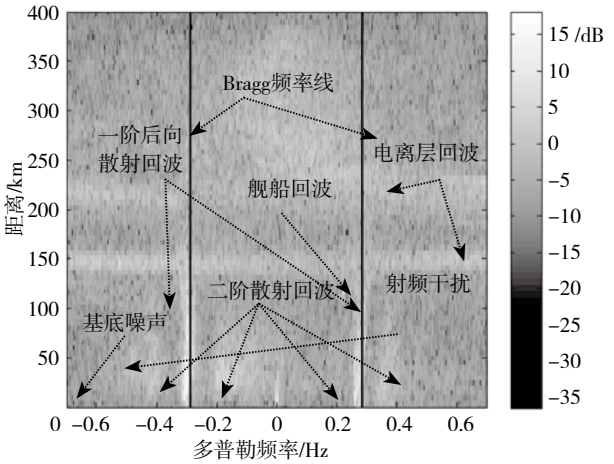

图2 OSMAR071接收的回波多普勒谱
(2008-07-28 T 12:00)

2.2 OSMAR071海面参数反演方法

高频地波雷达OSMAR071系统基于Barrick提出的海面与高频电磁波相互作用的一阶散射方程，利用深水重力波的色散关系进行海洋表面流信息的提取，利用单部雷达可以探测到径向流场，通过两部雷达对同一区域的照射，实现合成矢量流场；几次海上对比验证试验表明，OSMAR系列高频地波雷达海流探测已达到业务化运行水平(吴雄斌 等，2003)。

海面回波多普勒谱中左右一阶峰的高度差异与风向有着紧密的联系，Stewart和Barnum(1975)提出的SBM法给出了雷达回波多普勒谱左右一阶峰能量差与风向的关系模型：

$$R_d = 10\lg[\tan^s(|\theta_W|/2)] \quad (1)$$

式中，R_d表示左右一阶峰的能量差，s为风向扩展因子，表示海浪能量关于风向的分散程度，θ_W表示风向与雷达波束方向的夹角，由式(1)求解出来的风向为$\phi_W = \phi_0 \pm 2\arctan[10^{R/(10s)}]$，$\phi_0$表示雷达波束方向。该式中存在“±”号，表示了一种风向不确定性，即风向模糊性。其原因是风向与雷达波束方向夹角相同时雷达观测到的一阶海洋回波能量是等效的。Heron和Rose(1986)提出了多波束采样确定风向的方法，即在雷达观测的海域内假定海浪方向谱是近似均匀分布的，用一部雷达分别照射几个不同方向，根据不同方向的回波多普勒谱中两个一阶峰强度的不同比值R_d，推算出唯一合理的海面风向方位角θ_w和浪高方向谱中的扩展因子s。图3

给出了利用3个波束消除风向模糊性的示意图。

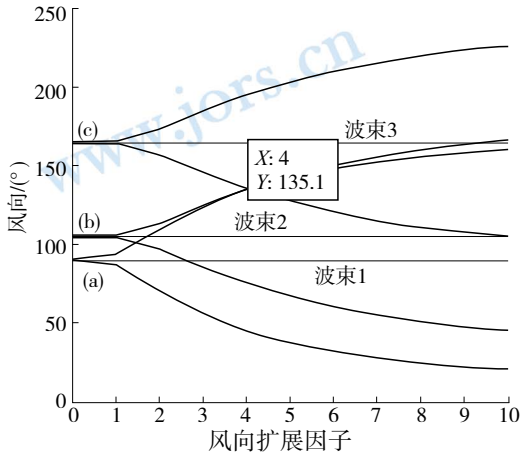

图3 三波束采样法消除风向模糊性示意图

海面回波谱中连续的二阶谱可以用来提取有效波高信息。Barrick(1977)提出了简单实用的工程应用方法。OSMAR071雷达采用改进的Barrick有效波高计算公式进行海面有效波高的反演，具体表述如下(Wu等，2009)：

$$h=\frac{\alpha}{k_0}(R-\mu)^{\beta} \tag{2}$$

式中，R表示二阶谱能量与一阶谱能量之比，k_0为雷达电波波数，α、β和μ为适应OSMAR071系统的模型参数，通过半年的试验观测分别标定为1.43、0.71和0.4，具体过程见文献(Wu 等，2009)。

由Sverdrup和Munk提出并由Bretschneider修正的方程式SMB关系式给出了风速与有效波高之间的关系(Dexter和Theodorides，1982)，见式(3)，可以利用此关系式通过非线性迭代来求取风速。

$$\frac{gH_S}{V_{10}^2}=0.26\tanh\left[\left(\frac{1}{f_m V_{10}}\right)^{3/2}\frac{(3.5g)^{3/2}}{10^2}\right] \tag{3}$$

式中，H_S表示海面有效波高，f_m表示波高谱峰值频率，U_{10}为海面10 m处的风速，g为重力加速度，取9.8 m/s^2。

3 遥测结果与分析

3.1 凤凰台风介绍

“凤凰”(FUNG-WONG)台风是2008年西北太平洋第8号台风，于(2008-07-25)下午14: 00在中国台湾以东洋面(130.6° E，21.6° N)生成，随后稳定向偏西北方向移动，25日16: 00加强为强热带风暴，并于26日下午加强为台风并稳定西行，27日20: 00加强为强台风，中心附近最大风力达45 m/s。28日上午06: 30前后在台湾省花莲县南部沿海登陆，并于28日晚上22: 00在福建省福清市东瀚镇再次登陆，随着台风继续向北偏东方向移动，进入山东省境内，强度逐渐减弱。

3.2 海面风、浪的雷达遥感

高频地波雷达OSMAR071位于福建省龙海，在“凤凰”台风7级风力半径内。在该台风进入台湾海峡至从福建福清登陆期间，雷达工作频率为7.82 MHz，对应的谐振一阶散射海浪波长为19 m，Bragg频率为0.28 Hz。雷达距离分辨率和角度分辨率分别为5 km和5° 。利用3(距离元) × 3(方位)=9个格点上的多普勒谱进行加权平均后的多普勒谱进行中间格点处的风、浪参数反演。图4和图5分别为2008年7月28日00: 00，6: 00，12: 00和18: 00四个时刻雷达输出的海面浪、风场分布，风速和波高探测距离可达100 km。图4中雷达探测海域的东北方向波高相对较大，这与台风中心位于雷达探测海域东北方向是一致的；雷达探测波高呈先上升后下降的趋势，这与台风先进入台湾海峡，之后从福建福清登陆的时间是一致的。由于台风是低气压，中间空气上升，旁边空气补充，空气受地球自转偏向力的影响呈逆时针气旋方式。雷达站位于台风中心西南方向，因此在台风中心经过台湾海峡北部期间，雷达探测海域的风向由北风逐渐向西北风转变，这与图4表现的风向特征是一致的；图5中风速表现的特征与波高特征是一致的。

3.3 探测精度分析

3.2节中的定性分析表明：OSMAR071海面探测结果符合台风期间的海面风、浪场变化特征。为了定量验证OSMAR071的风、浪探测精度，将雷达定点观测结果与附近大浮标实测风浪数据进行对比。图6和图7分别为“凤凰”台风期间雷达与浮标有效波高的时间序列对比图和散点图，二者相关系数为0.72，均方根误差为0.48 m。图8为风向和风速的矢量序列对比，图9对应为风矢量的散点图，风向的相关系数为0.97，均方根误差为27.7° ，风速的相关系数为0.6，均方根误差为3.5 m/s。7月29日12：00后由于浮标出现故障，风速数据未能获取。

从对比结果来看，台风雷达探测结果与浮标观测结果吻合度高，但是也存在一定程度的差异，造成这种差异的原因主要在于：(1)两种探测手段在空间上与时间上的取样方式不同。雷达是对几平方公里雷达面元中数十分钟时间长度内浪场数据的平均；浮标是

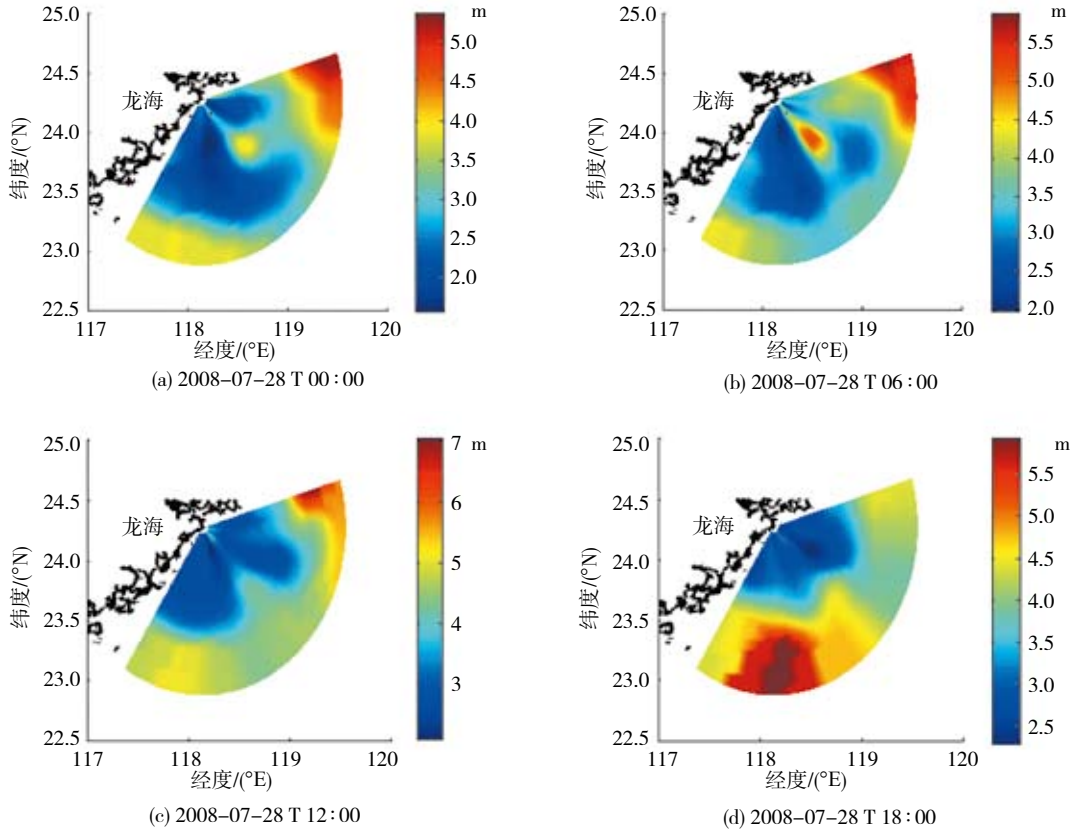

(a) 2008-07-28 T 00:00 (b) 2008-07-28 T 06:00

(c) 2008-07-28 T 12:00 (d) 2008-07-28 T 18:00

图4 “凤凰”台风期间OSMAR071遥感的海面波高

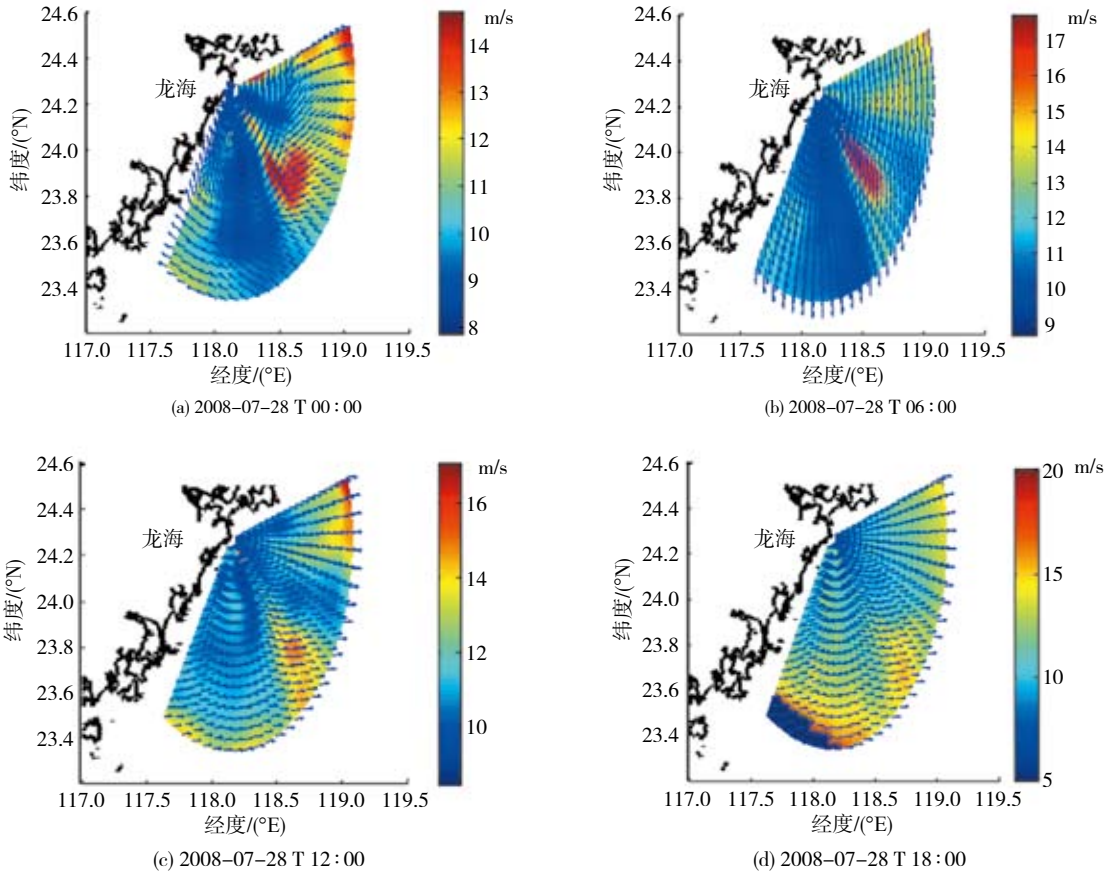

(a) 2008-07-28 T 00:00 (b) 2008-07-28 T 06:00

(c) 2008-07-28 T 12:00 (d) 2008-07-28 T 18:00

图5 “凤凰”台风期间OSMAR071遥感的海面风场

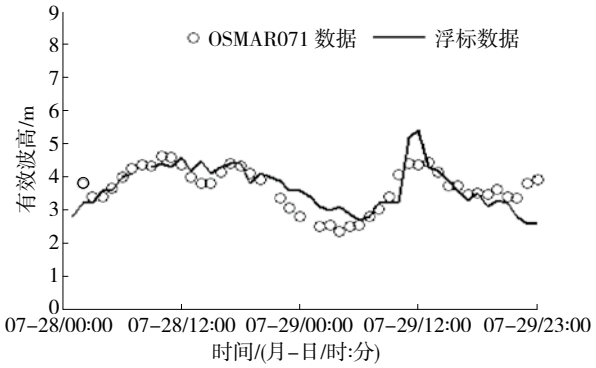

图6 定点浮标波高与雷达测量波高序列对比
(时间：2008-07-28—2008-07-29)

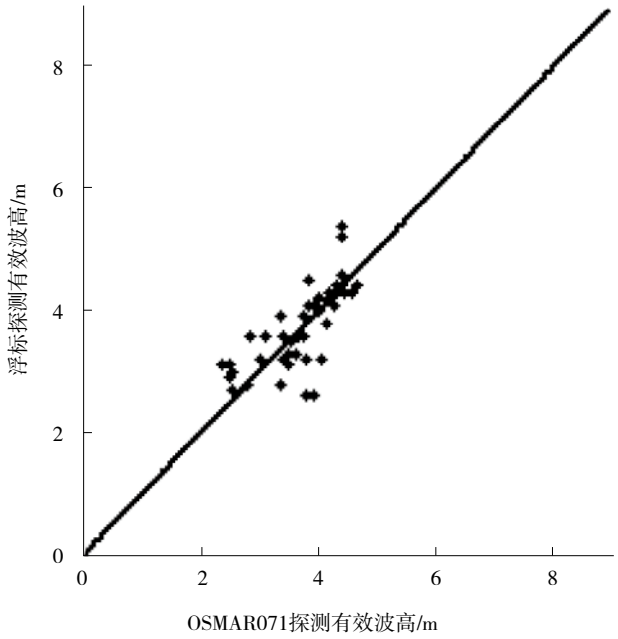

图7 图6波高序列对应的散点图

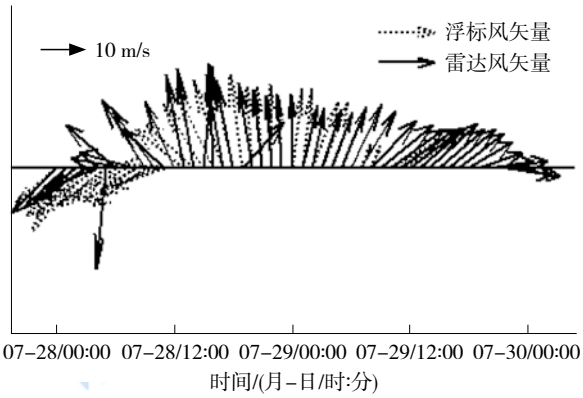

图8 定点浮标风向与雷达测量风矢量对比
(时间：2008-07-28—2008-07-29)

对其所处位置上局部波高的取样，这会导致雷达所测得的结果与浮标结果之间存在一定程度的差异。(2)复杂的电磁环境(射频干扰)、海上舰船等硬目标和电离层回波等会影响雷达观测结果。(3)在高海况下，高阶非线性作用较强，使得海洋回波谱一阶谱和二阶谱

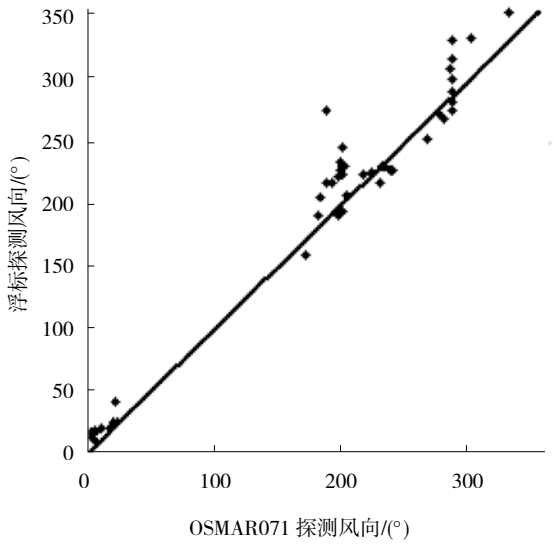

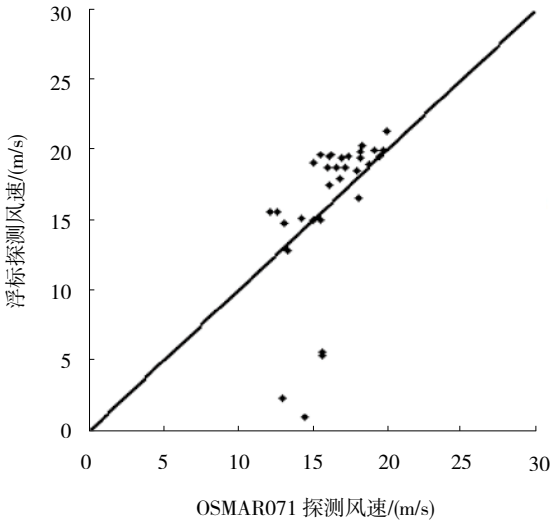

图9 图8风矢量序列风向、风速对应的散点图

的边界不易区分。(4)高频地波雷达反演有效波高和风速很大程度依赖于雷达回波谱中的二阶谱信噪比，天线的旁瓣波束会影响二阶谱。(5)回波谱处理过程中用于平均的格点数目，FFT谱分析，回波谱噪声基底的确定等都会对风浪参数的反演产生一定的影响。(6)风向反演模型为二元非线性方程，正负一阶峰能量的比率误差和风向扩展因子的误差都会影响风向探测精度。文中采用多个雷达波束方向的数据来消除风向模糊性，事实上不同波束方向的风向扩展因子会有差异，而且信噪比较低、外界射频干扰、舰船硬目标回波等都可能引起模糊性选择时出现误判，这些都会影响风向反演精度。图8中2008-07-28 21：00出现了一个风向反演异常点，是进行风向模糊性判断时误判导致的。从该海元回波多普勒谱上可以看出正负一阶谱出现较严重的谱分裂，可能是舰船等硬目标回波污染了一阶海洋回波，从而导致风向误判。

图9中浮标测量风速较小时，偏差较大是由于2008-

07-29上午4：00后浮标测量风速出现故障导致该时刻数据不可信引起的。事实上，在风速较小时，误差较大是低频段的地波雷达普遍存在的现象，主要原因包括：(1)HFSWR是通过对谐振海浪的遥感来测量海面动力学要素的，谐振海浪的波长为雷达电波波长的一半。在7.5—8.5 MHz频段，谐振海浪的波长为20 m左右，在较小风速情况下，这种波长的海浪无法得到足够的能量，不能充分发展，其回波相对较弱，且稳定性差，导致结果变差。(2)HFSWR海洋遥感机理表明，较低电波频率适合于高海况探测，高端电波频率适合于低海况探测，因此利用高、低端频率搭配来同时进行海面遥感，能解决部分低海况下的风、浪探测问题，但是高端频率电波的衰减大，导致探测距离会下降，覆盖区域有限。(3)风速较小时观测结果误差增加的另一个原因是非科学性的，即风浪小时，大量近海渔民船只出海，渔船本身及渔船间的高频无线电通信会造成干扰，降低结果的准确性。

4 结 论

高频地波雷达工作频率与其可探测的海浪频率范围直接相关，短波段低端电波频率适合于较高海况，而短波段高端电波频率适合于低海况。OSMAR071系统工作在7.5—8.5 MHz，属于短波段低端频率，对应谐振海浪的波长为20 m左右，该频段电波对海况级别较低的海浪不敏感，适合于高海况海洋环境的监测。相对来说，台风期间整个探测海域的海况级别较高，为进行高频地波雷达风浪探测研究创造了良好的条件。“凤凰”台风期间相关海域海面完整实时的风、浪监测，与浮标的风浪结果的对比可以看出，二者的吻合程度高，进一步证实了OSMAR071系统探测海洋表面风、浪的能力，这也是中国首次对台风期间风速和波高的大面积实时完整观测。相对于浮标只能探测到浮标所在位置处的单点波高、风向和风速等海洋表面动力学参数序列，高频地波雷达可以探测雷达波束覆盖100 km范围内的波高和风速，200 km范围内的风向，充分体现了地波雷达的优越性。高频地波雷达系统位于海岸，维护方便，不受恶劣天气影响，是一种良好的台风期间海面风浪遥感手段。

当前，高频地波雷达风、浪探测处于研究发展阶段，仅对一次台风的观测对比不能充分说明雷达探测风、浪的可靠性，还需进一步进行观测分析。另外，海面波高方向谱充分包含了海面风向、风速、波高、波向和波周期等海洋表面状态参量；雷达海面回波多普勒谱是海洋表面重力波与雷达电波相互作用产生的。因此，从雷达海面回波谱中提取海面波高方向谱(Lipa和Barrick，1986；Wyatt，1986；Howell和Walsh，1993；Hisaki，2009)，尤其是观测台风期间海面波高方向谱的变化，是今后要重点研究的内容。

志 谢 感谢厦门大学近海海洋环境国家重点实验室提供的浮标数据。

参考文献(References)

Barrick D E. 1977. Extraction of wave parameters from measured HF radar sea-echo Doppler spectra. Radio Science, 12(3): 415–424

Barrick D E. 2008. 30 Years of CMTC and CODAR. Proceedings of the IEEE/OES/CMTC Ninth Working Conference on Current Measurement Technology: 131–136

Barnes L. 1998. HF Radar-The Key to Efficient Wide Area Maritime Surveillance. EEZ Technology, Edition 3. London: ICG Publishing LTD: 115–118

Dexter P E and Theodorides S. 1982. Surface wind speed extraction from HF sky-wave radar Doppler spectra. Radio Science, 17(3): 643–652

Heron M L and Rose R J. 1986. On the application of HF ocean radar to the observation of temporal and spatial changes in wind direction. IEEE Journal of Oceanic Engineering, 11(2): 210–218 DOI: 10.1109/JOE.1986.1145173

Hisaki Y. 2009. Quality control of surface wave data estimated from low signal-to-noise ratio HF radar Doppler spectra.Journal of atmospheric and oceanic technology. 26: 2444–2661

Howell R and Walsh J. 1993. Measurement of ocean wave spectra using narrow-beam HF radar. IEEE Journal of Oceanic Engineering, 18(3): 296–305

Lipa B J and Barrick D E. 1986. Extraction of sea state from HF radar sea echo: mathematical theory and modeling, Radio Science, 21(1): 81–100 DOI: 10.1029/RS021i001p00081

Liu L, Wu X B, Chen F, Yang S L and Ke H Y. 2007. Algorithm for HF radar vector current measurements. Journal of Oceanography, 63(1): 47–66 DOI: 10.1029/RS021i001p00081

Stewart R H and Barnum J R. 1975. Radio measurements of oceanic winds at long ranges: an evaluation. Radio Science, 10(10): 853–857 DOI: 10.1029/RS010i010p00853

Wu X B, Li L, Shao Y X, Li Y and Guo T. 2009. Experimental determination of sinificant waveheight by OSMAR71: comparison with results from Buoy. Journal of Wuhan University Nature Science, 14(6): 499–504

吴雄斌，杨绍麟，程丰，吴世才，杨子杰，文必洋，石振华，田建生，侯杰昌，柯亨玉，高火涛. 2003. 高频地波雷达东海海洋表面矢量流探测试验. 地球物理学报，46(3): 340–346

Wyatt L R. 1986. The measurement of the ocean wave directional spectrum from HF radar doppler spectra. Radio Science, 21(3): 473–485